© 2022. Published by The Company of Biologists Ltd | Journal of Cell Science (2022) 135, jcs258745. doi:10.1242/jcs.258745

RESEARCH ARTICLE

More than two populations of microtubules comprise the dynamic mitotic spindle

Aaron R. Tipton and Gary J. Gorbsky*

ABSTRACT

The microtubules of the mitotic spindle mediate chromosome alignment to the metaphase plate, then sister chromatid segregation to the spindle poles in anaphase. Previous analyses of spindle microtubule kinetics utilizing fluorescence dissipation after photoactivation described two main populations, a slow and a fast turnover population, and these were ascribed as reflecting kinetochore versus non-kinetochore microtubules, respectively. Here, we test this categorization by disrupting kinetochores through depletion of the Ndc80 complex in U2OS cells. In the absence of functional kinetochores, microtubule dynamics still exhibit slow and fast turnover populations, although the proportion of each population and the timings of turnover are altered. Importantly, the data obtained following Hec1 (also known as Ndc80) depletion suggests that other subpopulations, in addition to kinetochore microtubules, contribute to the slow turnover population. Further manipulation of spindle microtubules revealed a complex landscape. For example, although Aurora B kinase functions to destabilize kinetochore bound microtubules it might also stabilize certain slow turnover non-kinetochore microtubules. Dissection of the dynamics of microtubule populations provides a greater understanding of mitotic spindle kinetics and insight into their roles in facilitating chromosome attachment, movement and segregation during mitosis.

KEY WORDS: Cell cycle, Chromosome, Fluorescence, Microtubules, Mitosis, Mitotic spindle

INTRODUCTION

The mitotic spindle is a highly dynamic, spatially organized array of microtubules and associated proteins that orchestrates equal distribution of the chromosomes to daughter cells. Microtubules comprising the mammalian mitotic spindle at metaphase are often broadly classified into three categories. Kinetochore fiber microtubules, which are heterogeneous in length, together comprise a dense bundle that extend from poles to kinetochores with many making direct contact with kinetochores at their plus ends. Kinetochore fiber microtubules play major roles in chromosome movement and in regulating the spindle checkpoint, sometimes termed the spindle assembly checkpoint, through interactions with kinetochores. Astral microtubules emanate from spindle poles with many extending toward the cell cortex where they are important for spindle positioning. Interpolar microtubules extend from the poles to interdigitate at the spindle equator and play critical roles in spindle structure. Early examination of internal spindle microtubule dynamics through fluorescence dissipation after photoactivation assays demonstrated that dissipation data were best fit by a double exponential curve (Zhai et al., 1995). Two populations of microtubules were detected, a fast turnover and a slow turnover population. These two populations were equated with non-kinetochore and kinetochore microtubules, respectively, which had been widely reported in early electron microscopic studies (Mastronarde et al., 1993; McIntosh et al., 1975; Rieder, 1981a,b, 1982; Salmon et al., 1976; Wise et al., 1991). However, judging from ultrastructure, spindle microtubules likely include more than two populations. For example, within kinetochore fibers, electron microscopy identifies microtubules that reach from pole to kinetochore, microtubules linked to either the pole or the kinetochore with the other end free, and microtubules with two free ends (McDonald et al., 1992; Rieder, 1981b). Potentially, all might exhibit different dynamics within the fiber. Additionally, microtubules that branch from kinetochore fibers and microtubules bridging sister kinetochore fibers have been observed within the mitotic spindle (Kajtez et al., 2016; Kamasaki et al., 2013; Mastronarde et al., 1993; Petry et al., 2013). To better evaluate the multiplicity of microtubule turnover within metaphase mitotic spindles, we carried out photoactivation experiments while manipulating populations of microtubules in U2OS cells.

RESULTS

Mitotic spindles in cells lacking functional kinetochores still reveal fast and slow turnover microtubule populations

Early fluorescence dissipation after photoactivation observations of spindle microtubule dynamics suggested that the slow turnover population of microtubules within the spindle comprised kinetochore fiber microtubules, as based on observations demonstrating they are more stable than non-kinetochore microtubules (Cassimeris et al., 1990; Gorbsky and Borisy, 1989; Mitchison, 1988; Rieder, 1981b; Salmon et al., 1976, 1984; Zhai et al., 1995). The Ndc80 complex, comprising Hec1 (also known as Ndc80), Nuf2, Spc24 and Spc25 is the primary end-on microtubule binding component at kinetochores (DeLuca et al., 2005, 2006; McCleland et al., 2004; Wei et al., 2007). Therefore, if only two populations, kinetochore and non-kinetochore microtubules, exist within the central spindle of metaphase cells, disruption of the Ndc80 complex should eliminate the slow turnover population.

To test this idea, we measured fluorescence dissipation after photoactivation of microtubules in metaphase U2OS cells stably expressing photoactivatable GFP (PAGFP)–α-tubulin and mCherry–α-tubulin. Cells transfected with either control or Hec1 siRNA, to prevent kinetochore–microtubule interaction, were analyzed. The proteasome inhibitor MG132 at 10 µM was included to prevent mitotic exit, since spindle checkpoint signaling is abrogated by robust inhibition of the Ndc80 complex

Cell Cycle and Cancer Biology Research Program, Oklahoma Medical Research Foundation, Oklahoma City, OK 73104, USA.

*Author for correspondence (GJG@omrf.org)

G.J.G., 0000-0003-3076-4725

Handling Editor: David Glover
Received 7 April 2021; Accepted 6 December 2021

Journal of Cell Science (2022) 135, jcs258745. doi:10.1242/jcs.258745

(McCleland et al., 2003). Only cells entering mitosis during the time frame of imaging were used because we determined that turnover of microtubules is significantly slowed over time when there is a prolonged metaphase arrest in cells treated with MG132 (Fig. S1), but not upon a brief arrest (see below). Mitotic spindles were located by mCherry–α-tubulin fluorescence. A bar-shaped region within the spindle on one side of the metaphase plate was photoactivated, and time-lapse images were acquired. Representative images depict fluorescence in pre- and post-photoactivated cells and the mid-volume mCherry–α-tubulin plane (Fig. 1A, top). As determined in previous photoactivation experiments with spindle microtubules (Zhai et al., 1995), data from control cells were best fit by double exponential curves with the formula:

$$F = A1 \times \exp(-k1 \times t) + A2 \times \exp(-k2 \times t), \quad (1)$$

where A1 and A2 represent the percentage of the total fluorescence contribution of the fast turnover and slow turnover microtubule populations, and k1 and k2 represent the respective decay rate constants (Fig. 1, bottom). However, even though Hec1 depletion largely eliminates end-on microtubule attachment at kinetochores, photoactivation data remained best fit by the double exponential suggesting that photoactivation still revealed slow and fast turnover populations of microtubules (Fig. 1A, bottom). Fitting to single and triple exponential curves resulted in poorer R^2 values (R^2<0.990). In all instances, the data were best fit by a double exponential curve whose R^2 value is reported in the figures. Hec1 depletion by siRNA sufficient to disrupt end-on kinetochore attachment to spindle microtubules was confirmed by comparing fluorescent DNA morphology to known Hec1 depletion phenotypes and by western blot analysis (Fig. S2) (DeLuca et al., 2005; Martin-Lluesma et al., 2002).

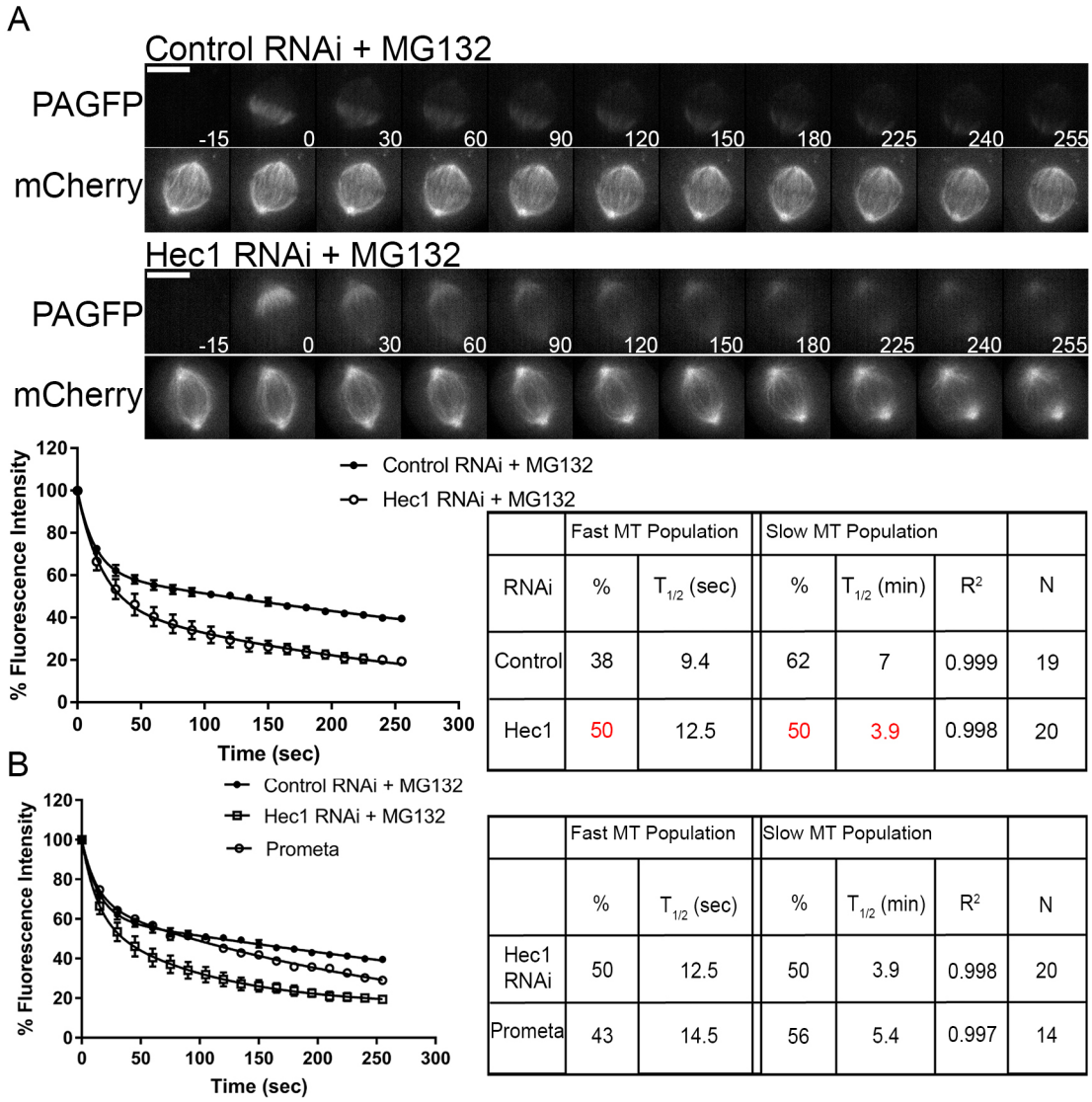

	Fast MT Population		Slow MT Population			
RNAi	%	$T_{1/2}$ (sec)	%	$T_{1/2}$ (min)	R^2	N
Control	38	9.4	62	7	0.999	19
Hec1	50	12.5	50	3.9	0.998	20

	Fast MT Population		Slow MT Population			
	%	$T_{1/2}$ (sec)	%	$T_{1/2}$ (min)	R^2	N
Hec1 RNAi	50	12.5	50	3.9	0.998	20
Prometa	43	14.5	56	5.4	0.997	14

Fig. 1. End-on attached microtubules comprise only a portion of the slow turnover microtubule population. (A) Top, select frames from live-cell imaging of tubulin photoactivation in metaphase U2OS cells stably expressing photoactivatable GFP–α-tubulin and mCherry–α-tubulin following transfection with either control or Hec1 siRNA and treatment with 10 µM MG132 to prevent mitotic exit. mCherry–α-tubulin frames are from the mid-volume plane. Only cells entering mitosis during imaging were photoactivated to ensure microtubule turnover was not affected by prolonged mitotic arrest. Time is given in seconds. Scale bars: 10 µm. Bottom, fluorescence dissipation after photoactivation. The filled and unfilled circles represent the mean±s.e.m. values recorded at each time point after photoactivation. Control, *n*=19 cells; Hec1, *n*=20 cells from three independent experiments. Lines indicate fitted curves (control RNAi R^2=0.999; Hec1 RNAi R^2=0.998). Significant differences (*P*<0.05; Mann–Whitney two-tailed *t*-test) in table from control indicated in red. (B) Analysis of prometaphase cells compared to Hec1 RNAi+MG132 and Control RNAi+MG132 treated cells. *n*=14 prometaphase cells from three independent experiments (R^2=0.997).

Journal of Cell Science (2022) 135, jcs258745. doi:10.1242/jcs.258745

Where the total fluorescence contribution of the fast and slow turnover microtubule populations in control cells was measured to be 38±2.4% and 62±2.3% (mean±s.e.m.), respectively, cells depleted of Hec1 had both a significant increase in the fast turnover population to 50%±4.2% and decrease in the slow turnover population to 50%±4.2%. Thus, in Hec1-depleted cells, the proportion in the slow turnover microtubule population is reduced, and the fast turnover population increased. This suggests that mitotic spindles in cells unable to form end-on microtubule attachments are still comprised of multiple populations, fast turnover and slow turnover. When microtubule half-lives were examined, minor changes were observed between control and Hec1-depleted cells in the fast turnover population. In contrast, the $t_{1/2}$ of the slow turnover population was significantly faster after Hec1 depletion ($t_{1/2}$=3.9±0.8 min; mean±s.e.m.) when compared with controls ($t_{1/2}$=7±0.6 min) (Fig. 1A, bottom). These data reveal the existence of one or more other slow populations that do not include kinetochore fiber microtubules with end-on attachments to kinetochores. Thus, contrary to the current assumptions regarding interpretation of photoactivation data, the mitotic spindle includes one or more populations with relatively slow turnover that are not end-on kinetochore bound. These might include microtubules stabilized by lateral interactions with kinetochores, by association with chromosome arms, or by parallel or antiparallel bundling. The broad spread of chromosomes along the spindle in Hec1-depleted cells partially resembles the somewhat less-dispersed array of chromosomes found at prometaphase. To compare with Hec1-depleted cells, we analyzed a set of prometaphase cells. Again, only cells that were observed to enter mitosis were used, and we did not add MG132 to avoid analyzing cells that might have completed prometaphase and entered anaphase during the observation window. Prometaphase cells exhibited fast and slow microtubule populations that were statistically similar to those of Hec-1 depleted cells (Fig. 1B). However, although the values from prometaphase cells trended toward those of Hec-1 depleted cells, their altered dynamics did not rise to the level of statistical significance when compared to that of metaphase cells (compare Fig. 1A with Fig. 1B). We speculate that the values in prometaphase cells may be a consequence of mixed populations of kinetochore fiber microtubules, a portion of which may have end-on attachments to kinetochores, and thus be different from the situation in Hec1-depleted cells where end-on attachments are likely to be largely absent.

Slow microtubule population turnover accelerates following loss of spindle bipolarity

Interpolar microtubules of opposite polarity that interdigitate plus ends near the spindle midline are another category of microtubules within the mitotic spindle. Early classification of the mitotic spindle structure suggested that most non-kinetochore microtubules were interpolar microtubules, concluding that interpolar microtubules constitute the bulk of the mitotic spindle (Mastronarde et al., 1993; McIntosh et al., 1975; Rieder, 1981a). Later, the fast turnover population of microtubules within the mitotic spindle was inferred to comprise interpolar microtubules (Zhai et al., 1995). To eliminate interdigitating interpolar microtubules, cells were treated with the Eg5 inhibitor S-trityl-L-cysteine (STLC) (10 µM) to block bipolar spindle formation, leaving microtubules extending from the unseparated centrosomes with uniform polarity, some of which are free in the cytoplasm while others interact with kinetochores or with chromosome arms. Cells were analyzed as described in Fig. 1. Representative images depict fluorescence in pre- and post-photoactivated cells and the mid-volume fluorescence mCherry–α-tubulin plane (Fig. 2, top). Whereas the total fluorescence contribution of the fast and slow turnover microtubule populations in control cells was measured to be 33±3.4% and 67±3.5% (mean±s.e.m.), respectively, cells treated with STLC had both a minor increase in the fast turnover microtubule population to 42±3.5% and a minor decrease in the slow turnover microtubule population to 58±3.4%. Thus, in cells treated with STLC, the proportion in the slow turnover microtubule population is reduced, resulting in an increase in the fast turnover population. In cells prevented from forming bipolar spindles (lacking interdigitating interpolar microtubules), microtubules still include fast and slow turnover populations. When microtubule half-lives were examined, no significant changes were observed between control and STLC-treated cells in the fast turnover population. In contrast, the $t_{1/2}$ of the slow turnover population was significantly faster following STLC treatment ($t_{1/2}$=3.3±0.3 min; mean±s.e.m.) when compared with controls ($t_{1/2}$=5.7±0.5 min) (Fig. 2, bottom). Contrary to previous assumptions, the data are consistent with the interpretation that interdigitating interpolar microtubules might also constitute a portion of the slow turnover population within the mitotic spindle. However, we cannot rule out that the faster $t_{1/2}$ of the slow turnover population might reflect changes in dynamic microtubules attached to kinetochores lacking bipolar attachment and tension, resulting in decreased stability. Similarly, increases in the proportion of astral microtubules may account for the minor increase in the fast turnover population.

We next sought to test whether the kinesin Eg5 (also known as KIF11) might function in regulating the dynamics of interpolar microtubules in bipolar metaphase cells. Cells were arrested at metaphase with MG132 then subsequently treated with DMSO or STLC. Consistent with previous observations in other cell lines, U2OS cells maintain biopolar spindles under these conditions, indicating that many cell types do not require Eg5 for maintenance of metaphase spindle bipolarity (Gayek and Ohi, 2014; Kollu et al., 2009). We did not observe a statistical difference in fast or slow microtubule $t_{1/2}$ between control MG132-arrested cells and MG132-arrested cells treated with STLC (Fig. S3) suggesting that Eg5 does not contribute to stabilization of interpolar microtubules.

Unfortunately, our efforts to simultaneously reduce both kinetochore-attached microtubules and interdigitating, interpolar microtubules were unsuccessful. Hec1-depleted cells treated with 100 µM of the Eg5 inhibitor Monastrol, formed bipolar spindles. Representative images depict fluorescence in pre- and post-photoactivated cells and the mid-volume fluorescence mCherry–α-tubulin and DNA plane (Fig. S4A). This finding suggests that functional end-on kinetochore attachments are required to collapse spindles in mitotic cells treated with Eg5 inhibitors. However, in a previous study, siRNA was used to deplete Nuf2, another component of the Ndc80 complex, and there, co-treatment with Eg5 inhibitor induced spindle collapse and formation of monopolar spindles (Ganem and Compton, 2004). We hypothesized that in the previous study, incomplete Nuf2 depletion may have left enough intact Ndc80 complex to produce partially functional end-on attached kinetochores. To test this hypothesis, we treated cells with low (20 nM) or high (100 nM) concentrations of Nuf2 siRNA. These cells were then treated with 100 µM Monastrol for 1 h, fixed and labeled for Nuf2, α-tubulin and with human anti-centromere antibody (ACA) by immunofluorescence. Cells were then scored for monopolar and bipolar spindles in each condition (Fig. S4B, left). In cells treated with the low concentration of Nuf2 siRNA, the majority (65%) were found to contain monopolar

Journal of Cell Science (2022) 135, jcs258745. doi:10.1242/jcs.258745

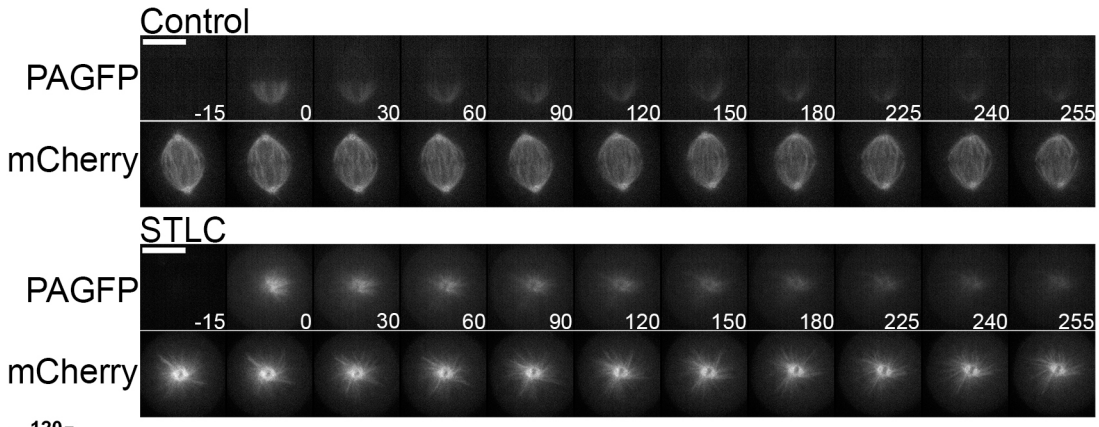

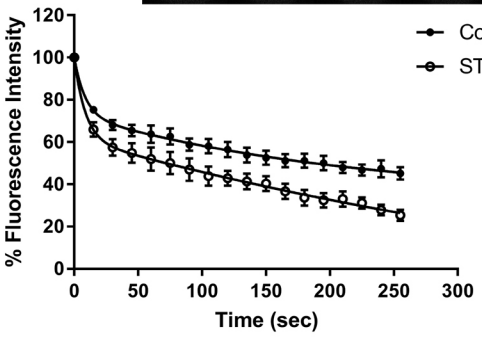

	Fast MT Population		Slow MT Population			
	%	$T_{1/2}$ (sec)	%	$T_{1/2}$ (min)	R^2	N
Control	33	9.8	67	5.7	0.997	16
STLC	42	7.2	58	3.3	0.997	18

Fig. 2. Interpolar microtubules also comprise a portion of the slow turnover microtubule population. Top, select frames from live-cell imaging of tubulin photoactivation in metaphase U2OS cells stably expressing photoactivatable GFP–α-tubulin and mCherry–α-tubulin following treatment with either control DMSO or 10 µM STLC to induce monopolar spindles. Cells were incubated 30 min prior to imaging. mCherry–α-tubulin frames are from the mid-volume plane. Only cells entering mitosis during imaging were photoactivated to ensure microtubule turnover was not affected by prolonged mitotic arrest. Control cells were imaged at metaphase. Time is given in seconds. Scale bars: 10 µm. Bottom, fluorescence dissipation after photoactivation. The filled and unfilled circles represent the mean±s.e.m. values recorded at each time point after photoactivation. Control n=16 cells, STLC n=18 cells from four independent experiments. Lines indicate fitted curves (control R^2=0.997; STLC R^2=0.997). Significant differences in table (P<0.05; Mann–Whitney two-tailed t-test) from control indicated in red.

spindles. In contrast, in cells treated with the high concentration of Nuf2 siRNA, a minority (23%) exhibited monopolar spindles. The minority population forming monopolar spindles in cells treated with the high concentration of Nuf2 siRNA displayed detectable levels of Nuf2 at kinetochores indicating incomplete knockdown even at the high concentration of siRNA (Fig. S4B). Live-cell imaging of cells entering mitosis following low and high Nuf2 siRNA treatment confirmed the above results (Movies 1 and 2). These data are consistent with our initial observation (Fig. S4A) and suggests that our Hec1 depletion more effectively eliminated microtubule attachment to kinetochores than did Nuf2 depletion.

To further characterize our depletions of Hec1 by siRNA, we measured levels of the spindle checkpoint protein, Mad2 (also known as MAD2L1) at kinetochores of mitotic cells. As demonstrated in previous studies with HeLa cells (DeLuca et al., 2003; Martin-Lluesma et al., 2002), depletion of Ndc80 components by siRNA in U2OS cells reduced, but did not eliminate, Mad2 accumulation at kinetochores of mitotic cells with intact microtubules and those in which microtubules were depolymerized by treatment with nocodazole (Fig. S4C). These results are consistent with the biphasic effects of Ndc80 complex inactivation on kinetochore–microtubule attachment and spindle checkpoint signaling. General inactivation of the complex disrupts microtubule attachment to kinetochores and induces a spindle checkpoint-dependent arrest in most cells, while a minority show checkpoint inactivation. Only more robust inactivation of the Ndc80 complex through antibody microinjection or siRNA combined with cell synchronization induces checkpoint abrogation in the majority of cells (McCleland et al., 2003; Meraldi et al., 2004).

We attempted to analyze spindle microtubule dynamics in monopolar spindles by inhibiting Eg5 in cells with partially reduced Ndc80 complex after treatment with the low concentration of Nuf2 siRNA. However, the fluorescence dissipation after photoactivation data obtained from these experiments resulted in extremely poor regression curve fits rendering the data uninterpretable (data not shown). We surmised that the partial inactivation of the Ndc80 complex led to variable effects on intact end-on microtubule attachment at kinetochores causing erratic variations in microtubule dynamics.

Turnover of both fast and slow microtubule populations is slower following temperature reduction

A well-established characteristic of spindle microtubules in cell culture models is the sensitivity of stability to changes in temperature (Brinkley and Cartwright, 1975; Rieder, 1981a,b; Zhai et al., 1995). In the LLC-PK cell line, decreases in temperature resulted in increases in the $t_{1/2}$ of the slow turnover microtubule population, with no major effect on the $t_{1/2}$ of the fast turnover population (Zhai et al., 1995). This study also reported an overall decrease in the fluorescence contribution of the fast turnover population and increase of the slow turnover population following reductions in temperature. We examined the effects of reductions in temperature on spindle microtubule dynamics in the U2OS cell line. Cells were imaged at 37°C (control) as described above or at room temperature (22–25°C; low temperature) as described in the

Journal of Cell Science (2022) 135, jcs258745. doi:10.1242/jcs.258745

Materials and Methods section. Representative images depict fluorescence in pre- and post-photoactivated cells and the mid-volume fluorescence mCherry–α-tubulin plane (Fig. 3, top). In contrast to a previous report (Zhai et al., 1995), we detected non-significant differences in the fluorescence contribution of fast and slow turnover microtubule populations when comparing control cells to cells imaged at low temperature. Substantial increases in $t_{1/2}$, indicating slower turnover, were observed in cells imaged at low temperature in both the fast turnover population (control $t_{1/2}$=7.1±0.6 s; low temperature $t_{1/2}$=15.7±1.2 s; mean±s.e.m.) and the slow turnover population (control $t_{1/2}$=4.7±0.5 min; low temperature $t_{1/2}$=14±1.1 min) (Fig. 3, bottom). This suggests that the $t_{1/2}$ of both populations detected are sensitive to a reduction of temperature. This is in contrast to the observations made by Zhai et al. (1995), which only reported a slower $t_{1/2}$ in the slow turnover microtubule population. One potential explanation for the discrepancies could be the difference in cell type. Additionally, advances in imaging technology may have permitted us to achieve higher temporal resolution allowing detection of a difference in $t_{1/2}$ of the fast turnover microtubule population.

Turnover of the slow microtubule population is reduced following Aurora B kinase inhibition

Aurora B kinase is an important regulator of kinetochore–microtubule attachment (Cheeseman et al., 2002; Cimini et al., 2006; Murata-Hori and Wang, 2002; Pinsky et al., 2006; Welburn et al., 2010). Aurora B responds to improper microtubule attachment to kinetochores by phosphorylating the N-terminal tail of Hec1/Ndc80, which reduces microtubule binding affinity. A previous report demonstrated in the PtK1 cell line that inhibition of Aurora B kinase activity via the small molecule ZM447439 caused an extensive increase (over 7-fold) in the $t_{1/2}$ of the slow turnover microtubule population, with no substantial effect on the $t_{1/2}$ of the fast turnover population when compared to control metaphase cells (Cimini et al., 2006). We examined the effects of Aurora B kinase inhibition on spindle microtubule dynamics in the U2OS cell line. To inhibit Aurora B kinase activity cells were treated with either 3 µM ZM447439 or DMSO (control) along with 10 µM MG132 to prevent mitotic exit. Cells were then analyzed as described above. Representative images depict fluorescence in pre- and post-photoactivated cells and the mid-volume fluorescence mCherry–α-tubulin plane (Fig. 4, top). No significant changes in the total fluorescence contributions of fast and slow turnover populations were observed between control cells and cells treated with ZM447439. When microtubule $t_{1/2}$ was examined, no significant changes in the fast turnover population were observed between control and ZM447439-treated cells. In contrast, the $t_{1/2}$ of the slow turnover population was significantly slower following ZM447439 treatment ($t_{1/2}$=13.9±0.7 min; mean±s.e.m.) when compared with controls ($t_{1/2}$=8.5±1.5 min) (Fig. 4, bottom). This change is consistent with inhibition of Aurora B inducing stabilization of kinetochore–microtubule attachments.

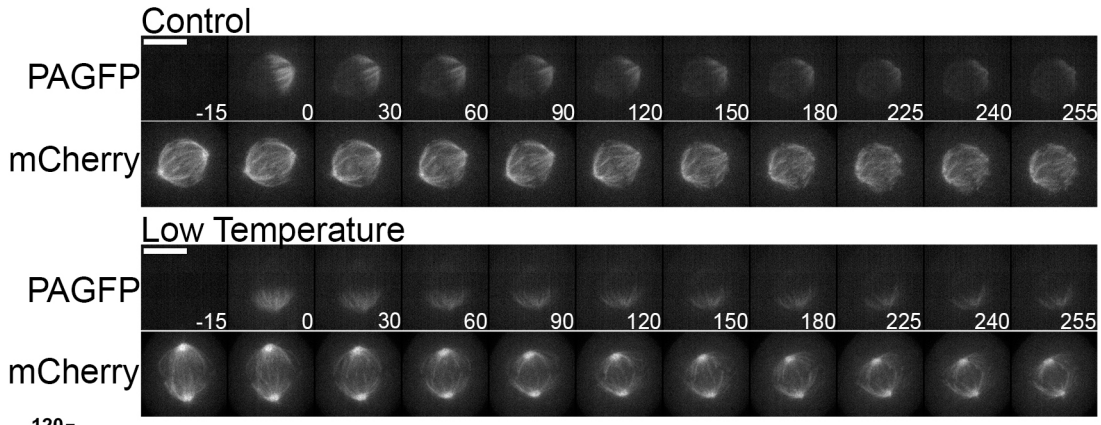

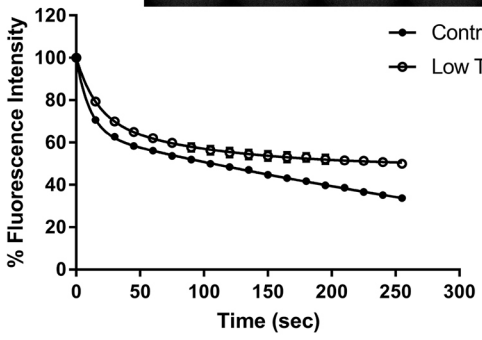

	Fast MT Population		Slow MT Population			
	%	$T_{1/2}$ (sec)	%	$T_{1/2}$ (min)	R^2	N
Control	35	7.1	65	4.7	0.999	19
Low Temp	38	15.7	62	14	0.998	22

Fig. 3. Both fast turnover and slow turnover microtubule populations are sensitive to decreases in temperature. Top, select frames from live-cell imaging of tubulin photoactivation in metaphase U2OS cells stably expressing photoactivatable GFP–α-tubulin and mCherry–α-tubulin following imaging at 37°C (standard conditions) or at low temperature (22–25°C; without a objective heater) by having an air curtain and medium warmed to room temperature. mCherry–α-tubulin frames are from the mid-volume plane. Only cells entering mitosis during imaging were photoactivated to ensure tubulin turnover was not affected by prolonged mitotic arrest. Cells were imaged at metaphase. Time is given in seconds. Scale bars: 10 µm. Bottom, fluorescence dissipation after photoactivation. The filled and unfilled circles represent the mean±s.e.m. values recorded at each time point after photoactivation. Control n=19 cells; low temperature n=22 cells from four independent experiments. Lines indicate fitted curves (control R^2=0.999; low temperature R^2=0.998). Significant differences in table (P<0.05; Mann–Whitney two-tailed t-test) from control indicated in red.

Journal of Cell Science (2022) 135, jcs258745. doi:10.1242/jcs.258745

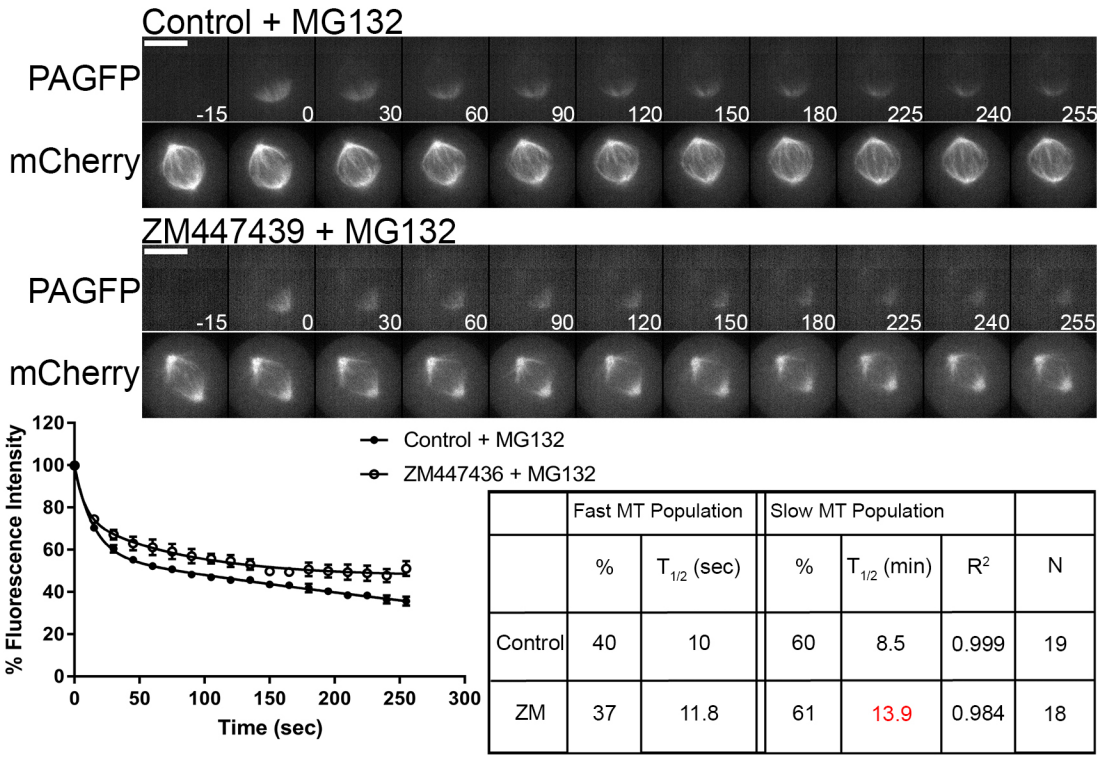

	Fast MT Population		Slow MT Population			
	%	$T_{1/2}$ (sec)	%	$T_{1/2}$ (min)	R^2	N
Control	40	10	60	8.5	0.999	19
ZM	37	11.8	61	13.9	0.984	18

Fig. 4. Aurora B kinase inhibition reduces turnover rate of slow microtubule population. Top, select frames from live-cell imaging of tubulin photoactivation in metaphase U2OS cells stably expressing photoactivatable GFP–α-tubulin and mCherry–α-tubulin following treatment with either control DMSO or 3 µM ZM447439 to inhibit Aurora B activity along with 10 µM MG132 treatment to prevent mitotic exit. Cells were incubated 30 min prior to imaging. mCherry–α-tubulin frames are from the mid-volume plane. Only cells entering mitosis during imaging were photoactivated to ensure microtubule turnover was not affected by prolonged mitotic arrest. Control cells were imaged at metaphase. Time is given in seconds. Scale bars: 10 µm. Bottom, fluorescence dissipation after photoactivation. The filled and unfilled circles represent the mean±s.e.m. values recorded at each time point after photoactivation. Control n=19 cells, ZM447439 n=18 cells from three independent experiments. Lines indicate fitted curves (Control R^2=0.999; ZM447439 R^2=0.984). Significant differences in table (P<0.05; Mann–Whitney two-tailed t-test) from control indicated in red.

Aurora B kinase may stabilize non end-on attached slow turnover microtubules

To further examine the role Aurora B kinase activity plays in regulating spindle microtubule dynamics during mitosis, Aurora B kinase activity was inhibited in cells depleted of Hec1/Ndc80. We hypothesized that if Aurora B solely regulated end-on attached kinetochore microtubules, then Aurora B inhibition should not alter spindle microtubule dynamics in cells depleted of functional kinetochores. To test this hypothesis, cells were transfected with control siRNA followed by DMSO treatment or Hec1 siRNA followed by 3 µM ZM447439 treatment and analyzed as described above. 10 µM MG132 was included to prevent mitotic exit. Representative images depict fluorescence in pre- and post-photoactivated cells and the mid-volume fluorescence mCherry–α-tubulin plane (Fig. 5, top). We did not detect significant changes in the proportion of the fast and slow turnover populations when comparing control-depleted and Hec1-depleted cells treated with Aurora kinase inhibitor. When microtubule $t_{1/2}$ times were examined, no significant changes were observed between control cells and cells depleted of Hec1 followed by ZM447439 treatment in the fast turnover population. However, the $t_{1/2}$ of the slow turnover population was significantly faster in cells depleted of Hec1 followed by ZM447439 treatment ($t_{1/2}$=2.2±0.3 min) when compared with controls ($t_{1/2}$=7.8±1.3 min) (Fig. 5, bottom). The $t_{1/2}$ of the slow turnover population in cells depleted of Hec1 followed by ZM447439 treatment was also faster when compared to cells depleted of Hec1 alone (Hec1 RNAi $t_{1/2}$=3.3±0.3 min; Hec1 RNAi+ZM447439 $t_{1/2}$=2.2±0.3 min). However, this effect was near but did not quite reach traditional statistical significance (P=0.0516). Taken together, these data suggest that Aurora B kinase can play roles in both stabilizing and destabilizing slow turnover microtubules within the mitotic spindle (comparing ZM447439 treatment alone and Hec1 depletion followed by ZM447439 treatment to their respective controls) (Fig. S5). One mechanism by which Aurora B kinase might play roles in stabilizing slow turnover microtubules is regulating the localization and activity of microtubule depolymerases, such as kinesin 13 family members (Andrews et al., 2004; Bakhoum et al., 2009; Knowlton et al., 2006, 2009; Lan et al., 2004; Ohi et al., 2003, 2004; Sampath et al., 2004). However, we cannot rule out other potential mechanisms by which Aurora B kinase functions in stabilizing slow turnover microtubule populations in cells lacking kinetochore attached microtubules. Fig. 6 is a compilation of all fluorescence dissipation after photoactivation data presented above with statistical analyses.

DISCUSSION

The mitotic spindle is essential in the equal distribution of genetic material during mitosis. Early studies examining spindle microtubule dynamics identified two distinct populations, a fast population that turns over in seconds and a slow population that turns over in minutes (Zhai et al., 1995). These two populations have come to be equated with non-kinetochore microtubules (comprising interdigitating interpolar microtubules and astral microtubules) and kinetochore microtubules (comprising microtubules attached to kinetochores), respectively. However, this assignment arose from observations

Journal of Cell Science (2022) 135, jcs258745. doi:10.1242/jcs.258745

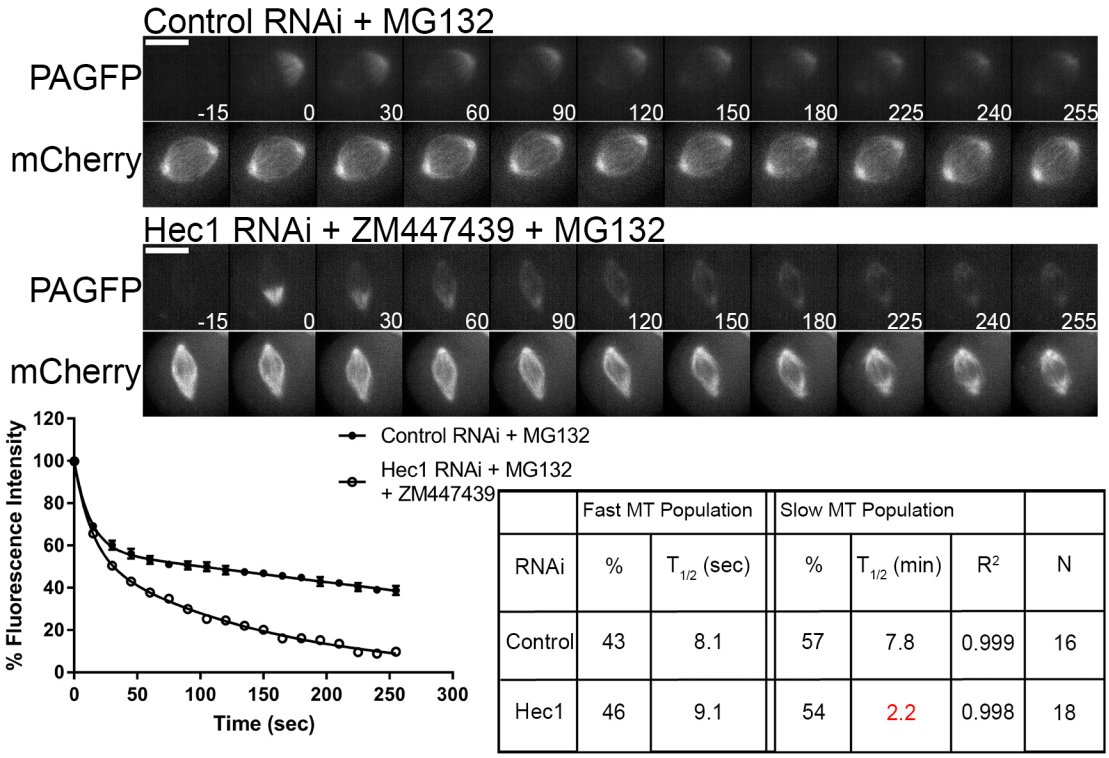

	Fast MT Population		Slow MT Population			
RNAi	%	$T_{1/2}$ (sec)	%	$T_{1/2}$ (min)	R^2	N
Control	43	8.1	57	7.8	0.999	16
Hec1	46	9.1	54	2.2	0.998	18

Fig. 5. Aurora B kinase inhibition increases turnover rate of slow microtubule population in cells depleted of end-on kinetochore–microtubule attachments. Top, select frames from live-cell imaging of tubulin photoactivation in metaphase U2OS cells stably expressing photoactivatable GFP–α-tubulin and mCherry–α-tubulin following transfection with either control or Hec1 siRNA along with 10 µM MG132 treatment to prevent mitotic exit followed by control DMSO or 3 µM ZM447439 to inhibit Aurora B activity. Cells were incubated 30 min prior to imaging. mCherry–α-tubulin frames are from the mid-volume plane. Only cells entering mitosis during imaging were photoactivated to ensure microtubule turnover was not affected by prolonged mitotic arrest. Control cells were imaged at metaphase. Time is given in seconds. Scale bars: 10 µm. Bottom, fluorescence dissipation after photoactivation. The filled and unfilled circles represent the mean±s.e.m. values recorded at each time point after photoactivation. Control n=16 cells, Hec1+ZM447439 n=18 cells from three independent experiments. Lines indicate fitted curves (Control RNAi R^2=0.999; Hec1 RNAi+ZM447439 R^2=0.998). Significant differences in table (P<0.05; Mann–Whitney two-tailed t-test) from control indicated in red.

indicating that microtubules attached to kinetochores displayed increased stability, whereas less-stable non-kinetochore microtubules represented the bulk of microtubules that constitute the mitotic spindle (Brinkley and Cartwright, 1975; Cassimeris et al., 1990; Gorbsky and Borisy, 1989; Mastronarde et al., 1993; McIntosh et al., 1975; Mitchison, 1988; Rieder, 1981a,b; Salmon et al., 1976, 1984; Zhai et al., 1995). In this study, we sought to determine whether this assumption reflected an oversimplification and whether mitotic spindle dynamics could be tracked through various manipulations to reveal multiple subpopulations. We targeted end-on attached kinetochore fibers by depleting Hec1/Ndc80. In cells depleted of this major microtubule-binding component at kinetochores, the slow turnover population was primarily affected, resulting in both a decrease in fluorescence contribution and a faster $t_{1/2}$ when compared to controls (Fig. 1). Data obtained following Hec1/Ndc80 depletion was best fit by a double exponential curve, indicating the persistence of multiple populations in the absence of end-on attached kinetochore microtubules. This suggests that end-on attached kinetochore fibers are not the sole population comprising slow turnover microtubules.

To target interdigitating interpolar microtubules, Eg5 inhibition was used to prevent bipolar spindle formation and formation of interdigitating interpolar microtubules. In contrast to previous assumptions suggesting that interpolar microtubules comprise the non-kinetochore (or fast turnover) population, we found that STLC treatment both decreased the fluorescence contribution and increased the $t_{1/2}$ of the slow turnover population when compared to controls (Fig. 2). However, we cannot rule out that the faster $t_{1/2}$ of the slow turnover population or the decrease in the slow turnover population may in part be due to microtubules interacting with kinetochores lacking bipolar attachment or tension, or with microtubules associating with chromosome arms. Analysis of monopolar spindles likely includes many free astral microtubules. Their increased addition to the rapid turnover population might result in a decrease in the slow turnover population. Additionally, we found Eg5 activity did not play a role in regulating spindle microtubule dynamics following the establishment of a bipolar spindle (Fig. S3).

When spindle microtubule dynamics were examined in conditions of reduced temperature, we found the $t_{1/2}$ of both the fast and slow turnover populations to be slower, with little change in the relative fluorescence contribution (Fig. 3). This was in contrast to previous observations reporting changes in the $t_{1/2}$ in the slow turnover population with no significant change in the $t_{1/2}$ in the fast turnover population (Zhai et al., 1995). These discrepancies could have been a result of a difference in cell type examined or advances in imaging technology. Finally, although we did note highly significant depression of microtubule turnover of both fast and slow populations dependent on reduced temperature, we cannot exclude that the changes may be indirect, due to general suppression of metabolic processes in the cells.

The well-recognized regulator of kinetochore–microtubule attachment, Aurora B kinase, was also analyzed for its role in regulating microtubule dynamics within the mitotic spindle. In partial agreement with a previous report (Cimini et al., 2006), we

Journal of Cell Science (2022) 135, jcs258745. doi:10.1242/jcs.258745

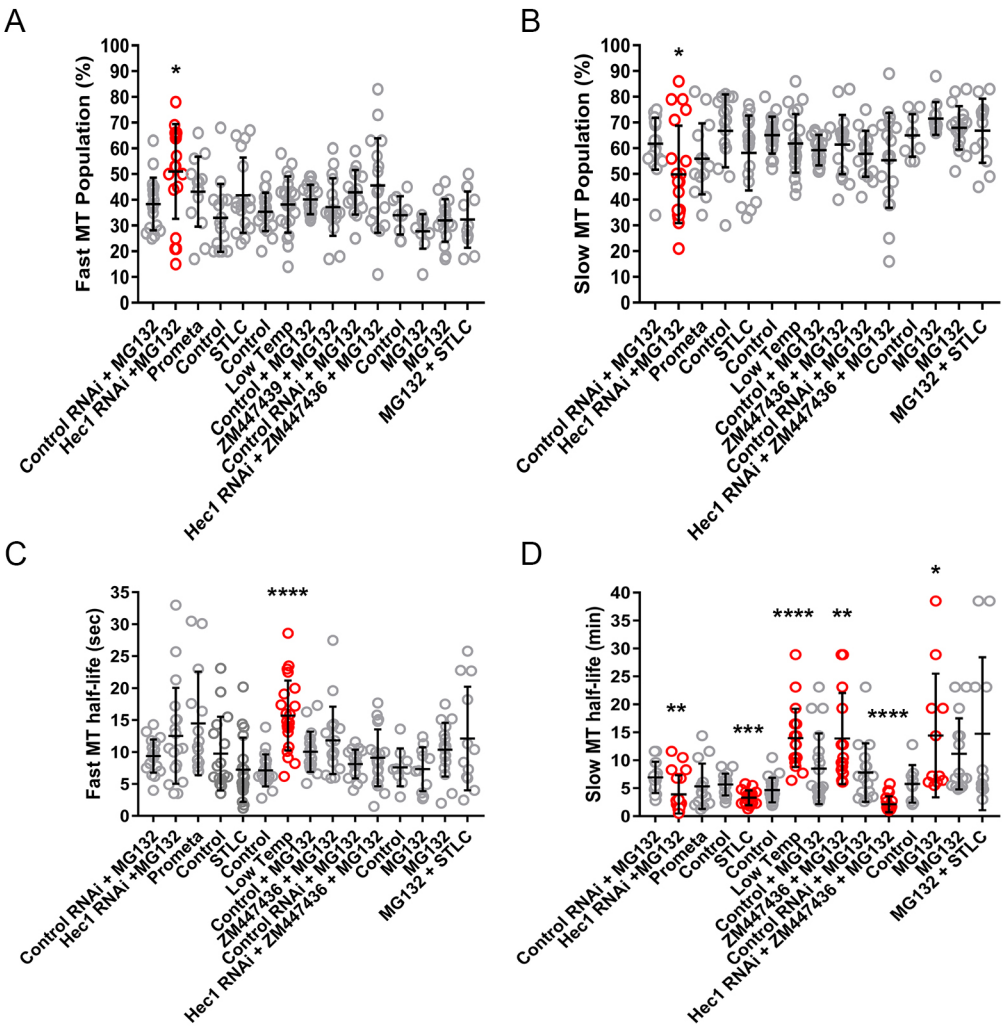

Fig. 6. Compilation of fluorescence dissipation after photoactivation data. Summary of (A) fast microtubule population data; (B) slow microtubule population data; (C) fast microtubule turnover data; (D) slow microtubule turnover data. Results are presented as mean±s.e.m. (n=14–22 cells) in pairs with experimental findings presented immediately following controls. Statistically significant changes in experimental versus control values are highlighted in red. *P<0.05; **P<0.01; ***P<0.001; ****P<0.0001 (determined by comparison to the appropriate experimental control with a Mann–Whitney two-tailed t-test).

found the $t_{1/2}$ of the slow turnover population was significantly slower following Aurora B kinase inhibition ($t_{1/2}$=13.9±0.7 min) compared to control ($t_{1/2}$=8.5±1.5 min). However, in contrast, the previous study, using the PtK1 cell line, reported extreme increases in stability for the slow turnover population with $t_{1/2}$ of 52.6 min at 3 µM ZM447439 and 230.0 min at 20 µM, compared to 7.4 min for control metaphase cells (Cimini et al., 2006). Increased stability of the slow turnover population upon Aurora B inhibition is consistent with the established role of Aurora B kinase in destabilizing microtubule–kinetochore attachments via phosphorylation of Hec1 (Cheeseman et al., 2002; Cimini et al., 2006; Murata-Hori and Wang, 2002; Pinsky et al., 2006; Welburn et al., 2010). In cells depleted of Hec1 and treated with Aurora B kinase inhibitor, the $t_{1/2}$ of the slow turnover population was somewhat increased. This suggests that although Aurora B kinase functions in destabilizing kinetochore–microtubule attachments, potentially it may conversely promote the stability of other, slow-turnover, populations within the mitotic spindle, perhaps through regulation microtubule depolymerases, such as those of the kinesin 13 family (Andrews et al., 2004; Bakhoum et al., 2009; Knowlton et al., 2006, 2009; Lan et al., 2004; Ohi et al., 2003, 2004; Sampath et al., 2004).

Together, this study demonstrates that turnover of microtubules within the mitotic spindle is significantly more complex than the previous two-component model suggests. The mitotic spindle likely comprises multiple subpopulations. The identity of the fast-turnover microtubule population within the mitotic spindle and mechanisms to manipulate its turnover (apart from reductions in temperature) remain elusive. Additionally, an inherent assumption made in this study is that spindle organization following various manipulations does not create new categories of microtubules. However, this might not be the case. For example in cells depleted of Hec1, non-K-fiber microtubules may assume an architecture that is not present in cells containing K-fibers. Testing this hypothesis will require more extensive manipulation of known microtubule-associated proteins and more precise methods to measure dynamics. Moreover, tubulin itself is also subject to post-translational modification (Barisic and Maiato, 2016; Barisic et al., 2015; Magiera and Janke, 2014; Song and Brady, 2015; Strzyz, 2016; Wloga et al., 2017; Yu et al., 2015). Examining how these various post-translational modifications play a role in regulating spindle microtubule dynamics during mitosis will be challenging but could lead to important insights into mitotic spindle assembly and function.

MATERIALS AND METHODS

siRNA

The siRNA sequence (5′-GAGUAGAACUAGAAUGUGA-3′) targeting Hec1 was synthesized by Qiagen. The ON-TARGETplus SMARTpool siRNA sequences (5′-GAACGAGUAACCACAAUUA-3′), (5′-UAGCU-GAGAUUGUGAUUCA-3′), (5′-GGAUUGCAAUAAAGUUCAA-3′), and (5′-AAACGAUAGUGCUGCAAGA-3′) targeting Nuf2 was synthesized by Dharmacon. Non-targeting control siRNA was synthesized by Bioneer.

Journal of Cell Science (2022) 135, jcs258745. doi:10.1242/jcs.258745

Cell culture, transfection, and drug treatments

U2OS cells stably expressing photoactivatable GFP–α-tubulin (PAGFP–α-tubulin) and mCherry–α-tubulin (see Acknowledgments) were cultured in Dulbecco's modified Eagle's medium (DMEM; Cytiva, cat. #SH30243.FS) with 10% fetal bovine serum (FBS; Biowest, cat. #S1620) supplemented with 100 IU penicillin and 100 µg/ml streptomycin (Corning, cat. #HOLO6), 20 mM HEPES (Caisson Laboratories, cat. #HOLO6), and 0.1 mM nonessential amino acids (NEAAs; Corning, cat. #25-025-CI) at 37°C with 5% CO_2. For siRNA transfection, cells were transfected with 50 nM (Hec1) or 20 nM or 100 nM (Nuf2) siRNA for 48 h using Lipofectamine RNAiMAX (Invitrogen; cat. #13-778-075) according to the manufacturer's protocol. To inhibit Aurora B activity, cells were treated with 3 µM ZM447439 (a gift from Dr Stephen Taylor, University of Manchester, Manchester, UK). 10 µM MG132 (Sigma-Aldrich, cat. #M7449-1ML) was also added to prevent mitotic exit. S-trityl-L-cysteine (STLC; Sigma-Aldrich, cat. #164739-5G) or Monastrol (Cayman Chemincal Co., cat. #15044-5) was used at 10 µM and 100 µM, respectively, to induce monopolar spindles. Taxol (Sigma-Aldrich, cat. #T7402-5MG) was used at 10 µM. All drugs were added 30 min, except where indicated, prior to imaging. SiR-DNA (Cytoskeleton, cat. #CY-SC007) was used at 500 nM to label DNA according to the manufacturer's protocol.

Photoactivation

PAGFP–α-tubulin- and mCherry–α-tubulin-expressing U2OS cells were grown on coverslips. To maintain appropriate pH levels and avoid evaporation during imaging, culture medium was exchanged to Leibovitz's L-15 medium supplemented with 10% FBS, 100 IU penicillin and 100 µg/ml streptomycin (Corning, cat. #30-002-CI), and the medium was overlaid with mineral oil. Cells were treated as detailed in the figure legends and imaged using a 100x, NA 1.4 objective on a Zeiss Axio Observer inverted microscope equipped with an objective heater, air curtain, Yokogawa CSU-22 (Yokogawa) spinning disk, Mosaic (digital mirror device, Photonic Instruments/Andor), a Hamamatsu ORCA-Flash4.0LT (Hamamatsu Photonics) and Slidebook software (Intelligent Imaging Innovations). Photoactivation was achieved by targeting a selected area with filtered light from the HBO 100 via the Mosaic, and confocal GFP images [19 *Z*-planes across 8 µm (0.5 µm/plane)] were acquired at 15 s intervals for ∼5 min. mCherry and SiR-DNA images were acquired at the mid-volume *Z*-plane. Only cells entering mitosis during imaging were photoactivated to ensure tubulin turnover was not affected by extended mitotic arrest. To quantify fluorescence dissipation after photoactivation, we measured pixel intensities within an area surrounding the region of highest fluorescence intensity and background subtracted using an area from the nonactivated half spindle using MetaMorph software. The values were corrected for photobleaching by determining the percentage of fluorescence loss during image acquisition after photoactivation in the presence of 10 µM taxol. Fluorescence values were normalized to the first time-point after photoactivation for each cell and the average intensity at each time point was fit to a double exponential curve $F=A1\times\exp(-k1\times t)+A2\times\exp(-k2\times t)$, using SigmaPlot (SYSTAT Software), where A1 and A2 represent the fast turnover and slow turnover microtubule populations with decay rates of k1 and k2, respectively. *t* is the time after photoactivation. The turnover half-life for each population of microtubules was calculated as ln2/k. *XY* scatter plots were generated using GraphPad Prism. The Mann–Whitney two-tailed *t*-test in Prism (GraphPad Software) was used to determine statistical significance among groups.

Immunofluorescence

PAGFP–α-tubulin- and mCherry–α-tubulin-expressing U2OS cells were grown on glass coverslips and treated as detailed in the figure legends. Cells were fixed in 2% paraformaldehyde in PHEM solution (60 mM PIPES, pH 6.9, 25 mM HEPES, 10 mM EGTA, 4 mM $MgSO_4$; components sourced from Calbiochem) containing 0.5% Triton X-100 for 15 min. Coverslips were washed in MBST (10 mM MOPS, 150 mM NaCl, 0.05% Tween 20; components sourced from Sigma-Aldrich and EMD-Millepore), blocked in 20% boiled normal goat serum (BNGS), and incubated overnight with primary antibodies. Samples were then incubated with secondary antibodies for 1 h, stained with DNA dye DAPI and mounted using Vectashield (Vector Laboratories). The following primary antibodies were used: rat anti-α-tubulin (YL1-2, 1:1000, Bio-Rad, cat. #MCA77G), rabbit anti-Nuf2 (1:500; a gift from P. Todd Stukenberg; University of Virginia, Charlottesville, USA), rabbit anti-XMad2 (1:500; a gift from Ted Salmon, University of North Carolina, Chapel Hill, USA) and human anti-centromere antibody (ACA; Antibodies Incorporated, cat. #15-134). Secondary antibodies used were goat anti-rabbit-IgG antibodies conjugated fluorescein isothiocyanate (FITC; Jackson ImmunoResearch), goat anti-rat-IgG antibodies conjugated to Cy3 (Jackson ImmunoResearch), and goat anti-human-IgG antibodies conjugated to Cy5 (Jackson ImmunoResearch). The images were acquired using a Zeiss Axioplan II microscope equipped with a 100×, NA 1.4 objective and a Hamamatsu ORCA-ER camera (Hamamatsu Photonics) and processed using MetaMorph software. Quantification of immunofluorescence images was performed as previously described (Daum et al., 2009).

Live-cell imaging

PAGFP–α-tubulin- and mCherry–α-tubulin-expressing U2OS cells were grown on glass coverslips. To maintain appropriate pH levels and avoid evaporation during imaging, the culture medium was exchanged to Leibovitz's L-15 medium supplemented with 10% FBS, penicillin, and streptomycin (as above), and the medium was overlaid with mineral oil. Cells were treated as detailed in figure legends. Time-lapse fluorescence images were collected using 100×, NA 1.4 objective on a Zeiss Axio Observer inverted microscope equipped with an objective heater, air curtain, Yokogawa CSU-22 (Yokogawa) spinning disk, Mosaic (digital mirror device, Photonic Instruments/Andor), a Hamamatsu ORCA-Flash4.0LT (Hamamatsu Photonics), and Slidebook software (Intelligent Imaging Innovations).. Images were captured every 3 min. Time-lapse videos displaying the elapsed time between consecutive frames were assembled using MetaMorph software.

Western blot analysis

For cell lysates, cells were arrested for 12 h with 100 ng/ml Nocodozole (Sigma-Aldrich, cat. #M1404-2MG) and mitotic cells were collected then lysed in cell lysis buffer [1× PBS, 0.5% NP-40, 1 µM tris(2-carboxyethyl)phosphine, and 10% glycerol] supplemented with protease inhibitor cocktail (Sigma-Aldrich) and phosphatase inhibitors [100 mM NaF (Sigma-Aldrich, cat. #S-1504), 1 mM Na_3VO_4 (Sigma-Aldrich, cat. #S-6508), 60 mM β-glycerophosphate (Sigma-Aldrich, cat. #G6376-100G) and 100 nM microcystin-LR (Sigma-Aldrich, cat. #457815-500UGM)]. The protein concentration of lysates was measured using the BCA Protein Assay kit (Thermo Fisher Scientific). For electrophoresis, sample loading buffer (Invitrogen) and DTT to a final concentration of 50 mM were added. Proteins were separated with a NuPAGE gel electrophoresis system (Invitrogen) and transferred to a 0.45-µm PVDF membrane (Immobilon-FL; EMD Millipore). Membranes were blocked in 10% SEA BLOCK blocking buffer (Thermo Fisher Scientific) and 0.05% Tween-20 in 1× PBS (PBST). The following primary antibodies were used: rabbit anti-Hec1 (1:1000; a gift from P. Todd Stukenberg), mouse anti-actin (1:1000; Abcam, cat. #ab6276). Membranes were washed in PBST. Secondary goat anti-mouse-IgG and goat anti-rabbit-IgG antibodies were conjugated to either IR700 or IR800 dyes (Azure Biosystems). Western blots were imaged on an Azure c600 Imaging System.

Acknowledgements

We thank, Marvin Tanenbaum, Rene Medema, and Helder Maiato for providing the U2OS cell line used, P. Todd Stukenberg and Ted Salmon for antibodies, Stephen Taylor for ZM447439 reagent and John R. Daum for technical assistance.

Competing interests

The authors declare no competing or financial interests.

Author contributions

Conceptualization: A.R.T., G.J.G.; Methodology: A.R.T.; Validation: A.R.T., G.J.G.; Formal analysis: A.R.T.; Investigation: A.R.T.; Resources: G.J.G.; Data curation: A.R.T.; Writing - original draft: A.R.T.; Writing - review & editing: G.J.G.;

Visualization: A.R.T.; Supervision: G.J.G.; Project administration: G.J.G.; Funding acquisition: G.J.G.

Funding
This work was supported by the National Institute of General Medical Sciences (grant 5R35GM126980). Deposited in PMC for release after 12 months.

Peer review history
The peer review history is available online at https://journals.biologists.com/jcs/article-lookup/doi/10.1242/jcs.258745.

References

Andrews, P. D., Ovechkina, Y., Morrice, N., Wagenbach, M., Duncan, K., Wordeman, L. and Swedlow, J. R. (2004). Aurora B regulates MCAK at the mitotic centromere. *Dev. Cell* **6**, 253-268. doi:10.1016/S1534-5807(04)00025-5

Bakhoum, S. F., Thompson, S. L., Manning, A. L. and Compton, D. A. (2009). Genome stability is ensured by temporal control of kinetochore-microtubule dynamics. *Nat. Cell Biol.* **11**, 27-35. doi:10.1038/ncb1809

Barisic, M. and Maiato, H. (2016). The tubulin code: a navigation system for chromosomes during mitosis. *Trends Cell Biol.* **26**, 766-775. doi:10.1016/j.tcb.2016.06.001

Barisic, M., Sousa, R. S. E., Tripathy, S. K., Magiera, M. M., Zaytsev, A. V., Pereira, A. L., Janke, C., Grishchuk, E. L. and Maiato, H. (2015). Microtubule detyrosination guides chromosomes during mitosis. *Science* **348**, 799-803. doi:10.1126/science.aaa5175

Brinkley, B. R. and Cartwright, J.Jr. (1975). Cold-labile and cold-stable microtubules in the mitotic spindle of mammalian cells. *Ann. N. Y. Acad. Sci.* **253**, 428-439. doi:10.1111/j.1749-6632.1975.tb19218.x

Cassimeris, L., Rieder, C. L., Rupp, G. and Salmon, E. D. (1990). Stability of microtubule attachment to metaphase kinetochores in Ptk1 cells. *J. Cell Sci.* **96**, 9-15. doi:10.1242/jcs.96.1.9

Cheeseman, I. M., Anderson, S., Jwa, M., Green, E. M., Kang, J.-S., Yates, J. R., Chan, C. S. M., Drubin, D. G. and Barnes, G. (2002). Phospho-regulation of kinetochore-microtubule attachments by the aurora kinase Ipl1p. *Cell* **111**, 163-172. doi:10.1016/S0092-8674(02)00973-X

Cimini, D., Wan, X., Hirel, C. B. and Salmon, E. D. (2006). Aurora kinase promotes turnover of kinetochore microtubules to reduce chromosome segregation errors. *Curr. Biol.* **16**, 1711-1718. doi:10.1016/j.cub.2006.07.022

Daum, J. R., Wren, J. D., Daniel, J. J., Sivakumar, S., McAvoy, J. N., Potapova, T. A. and Gorbsky, G. J. (2009). Ska3 is required for spindle checkpoint silencing and the maintenance of chromosome cohesion in mitosis. *Curr. Biol.* **19**, 1467-1472. doi:10.1016/j.cub.2009.07.017

DeLuca, J. G., Howell, B. J., Canman, J. C., Hickey, J. M., Fang, G. and Salmon, E. D. (2003). Nuf2 and Hec1 are required for retention of the checkpoint proteins Mad1 and Mad2 to kinetochores. *Curr. Biol.* **13**, 2103-2109. doi:10.1016/j.cub.2003.10.056

DeLuca, J. G., Dong, Y. M., Hergert, P., Strauss, J., Hickey, J. M., Salmon, E. D. and McEwen, B. F. (2005). Hec1 and Nuf2 are core components of the kinetochore outer plate essential for organizing microtubule attachment sites. *Mol. Biol. Cell* **16**, 519-531. doi:10.1091/mbc.e04-09-0852

DeLuca, J. G., Gall, W. E., Ciferri, C., Cimini, D., Musacchio, A. and Salmon, E. D. (2006). Kinetochore microtubule dynamics and attachment stability are regulated by Hec1. *Cell* **127**, 969-982. doi:10.1016/j.cell.2006.09.047

Ganem, N. J. and Compton, D. A. (2004). The KinI kinesin Kif2a is required for bipolar spindle assembly through a functional relationship with MCAK. *J. Cell Biol.* **166**, 473-478. doi:10.1083/jcb.200404012

Gayek, A. S. and Ohi, R. (2014). Kinetochore-microtubule stability governs the metaphase requirement for Eg5. *Mol. Biol. Cell* **25**, 2051-2060. doi:10.1091/mbc.e14-03-0785

Gorbsky, G. J. and Borisy, G. G. (1989). Microtubules of the kinetochore fiber turn over in metaphase but not in anaphase. *J. Cell Biol.* **109**, 653-662. doi:10.1083/jcb.109.2.653

Kajtez, J., Solomatina, A., Novak, M., Polak, B., Vukušić, K., Rüdiger, J., Cojoc, G., Milas, A., Šumanovac Šestak, I., Risteski, P. et al. (2016). Overlap microtubules link sister k-fibres and balance the forces on bi-oriented kinetochores. *Nat. Commun.* **7**, 10298. doi:10.1038/ncomms10298

Kamasaki, T., O'Toole, E., Kita, S., Osumi, M., Usukura, J., McIntosh, J. R. and Goshima, G. (2013). Augmin-dependent microtubule nucleation at microtubule walls in the spindle. *J. Cell Biol.* **202**, 25-33. doi:10.1083/jcb.201304031

Knowlton, A. L., Lan, W. J. and Stukenberg, P. T. (2006). Aurora B is enriched at merotelic attachment sites, where it regulates MCAK. *Curr. Biol.* **16**, 1705-1710. doi:10.1016/j.cub.2006.07.057

Knowlton, A. L., Vorozhko, V. V., Lan, W., Gorbsky, G. J. and Stukenberg, P. T. (2009). ICIS and Aurora B coregulate the microtubule depolymerase Kif2a. *Curr. Biol.* **19**, 758-763. doi:10.1016/j.cub.2009.03.018

Kollu, S., Bakhoum, S. F. and Compton, D. A. (2009). Interplay of microtubule dynamics and sliding during bipolar spindle formation in mammalian cells. *Curr. Biol.* **19**, 2108-2113. doi:10.1016/j.cub.2009.10.056

Lan, W., Zhang, X., Kline-Smith, S. L., Rosasco, S. E., Barrett-Wilt, G. A., Shabanowitz, J., Hunt, D. F., Walczak, C. E. and Stukenberg, P. T. (2004). Aurora B phosphorylates centromeric MCAK and regulates its localization and microtubule depolymerization activity. *Curr. Biol.* **14**, 273-286. doi:10.1016/j.cub.2004.01.055

Magiera, M. M. and Janke, C. (2014). Post-translational modifications of tubulin. *Curr. Biol.* **24**, R351-R354. doi:10.1016/j.cub.2014.03.032

Martin-Lluesma, S., Stucke, V. M. and Nigg, E. A. (2002). Role of Hec1 in spindle checkpoint signaling and kinetochore recruitment of Mad1/Mad2. *Science* **297**, 2267-2270. doi:10.1126/science.1075596

Mastronarde, D. N., Mcdonald, K. L., Ding, R. and Mcintosh, J. R. (1993). Interpolar Spindle Microtubules in Ptk Cells. *J. Cell Biol.* **123**, 1475-1489. doi:10.1083/jcb.123.6.1475

McCleland, M. L., Gardner, R. D., Kallio, M. J., Daum, J. R., Gorbsky, G. J., Burke, D. J. and Stukenberg, P. T. (2003). The highly conserved Ndc80 complex is required for kinetochore assembly, chromosome congression, and spindle checkpoint activity. *Genes Dev.* **17**, 101-114. doi:10.1101/gad.1040903

McCleland, M. L., Kallio, M. J., Barrett-Wilt, G. A., Kestner, C. A., Shabanowitz, J., Hunt, D. F., Gorbsky, G. J. and Stukenberg, P. T. (2004). The vertebrate Ndc80 complex contains Spc24 and Spc25 homologs, which are required to establish and maintain kinetochore-microtubule attachment. *Curr. Biol.* **14**, 131-137. doi:10.1016/j.cub.2003.12.058

McDonald, K. L., O'Toole, E. T., Mastronarde, D. N. and McIntosh, J. R. (1992). Kinetochore microtubules in PTK cells. *J. Cell Biol.* **118**, 369-383. doi:10.1083/jcb.118.2.369

McIntosh, J. R., Cande, W. Z. and Snyder, J. A. (1975). Structure and physiology of the mammalian mitotic spindle. *Soc. Gen. Physiol. Ser.* **30**, 31-76.

Meraldi, P., Draviam, V. M. and Sorger, P. K. (2004). Timing and checkpoints in the regulation of mitotic progression. *Dev. Cell* **7**, 45-60. doi:10.1016/j.devcel.2004.06.006

Mitchison, T. J. (1988). Microtubule dynamics and kinetochore function in mitosis. *Annu. Rev. Cell Biol.* **4**, 527-545. doi:10.1146/annurev.cb.04.110188.002523

Murata-Hori, M. and Wang, Y.-L. (2002). The kinase activity of aurora B is required for kinetochore-microtubule interactions during mitosis. *Curr. Biol.* **12**, 894-899. doi:10.1016/S0960-9822(02)00848-5

Ohi, R., Coughlin, M. L., Lane, W. S. and Mitchison, T. J. (2003). An inner centromere protein that stimulates the microtubule depolymerizing activity of a KinI kinesin. *Dev. Cell* **5**, 309-321. doi:10.1016/S1534-5807(03)00229-6

Ohi, R., Sapra, T., Howard, J. and Mitchison, T. J. (2004). Differentiation of cytoplasmic and meiotic spindle assembly MCAK functions by aurora B-dependent phosphorylation. *Mol. Biol. Cell* **15**, 2895-2906. doi:10.1091/mbc.e04-02-0082

Petry, S., Groen, A. C., Ishihara, K., Mitchison, T. J. and Vale, R. D. (2013). Branching microtubule nucleation in xenopus egg extracts mediated by augmin and TPX2. *Cell* **152**, 768-777. doi:10.1016/j.cell.2012.12.044

Pinsky, B. A., Kung, C., Shokat, K. M. and Biggins, S. (2006). The Ipl1-Aurora protein kinase activates the spindle checkpoint by creating unattached kinetochores. *Nat. Cell Biol.* **8**, 78-83. doi:10.1038/ncb1341

Rieder, C. L. (1981a). Effect of Hypothermia (20-25°C) on Mitosis in Ptk1 Cells. *Cell Biol. Int. Rep.* **5**, 563-573. doi:10.1016/S0309-1651(81)80007-0

Rieder, C. L. (1981b). The structure of the cold-stable kinetochore fiber in metaphase PtK1 cells. *Chromosoma* **84**, 145-158. doi:10.1007/BF00293368

Rieder, C. L. (1982). The formation, structure, and composition of the mammalian kinetochore and kinetochore fiber. *Int. Rev. Cytol. A Survey Cell Biol.* **79**, 1-58. doi:10.1016/S0074-7696(08)61672-1

Salmon, E. D., Goode, D., Maugel, T. K. and Bonar, D. B. (1976). Pressure-induced depolymerization of spindle microtubules III. Differential Stability in Hela-Cells. *J. Cell Biol.* **69**, 443-454. doi:10.1083/jcb.69.2.443

Salmon, E. D., McKeel, M. and Hays, T. (1984). Rapid rate of tubulin dissociation from microtubules in the mitotic spindle in vivo measured by blocking polymerization with colchicine. *J. Cell Biol.* **99**, 1066-1075. doi:10.1083/jcb.99.3.1066

Sampath, S. C., Ohi, R., Leismann, O., Salic, A., Pozniakovski, A. and Funabiki, H. (2004). The chromosomal passenger complex is required for chromatin-induced microtubule stabilization and spindle assembly. *Cell* **118**, 187-202. doi:10.1016/j.cell.2004.06.026

Song, Y. and Brady, S. T. (2015). Post-translational modifications of tubulin: pathways to functional diversity of microtubules. *Trends Cell Biol.* **25**, 125-136. doi:10.1016/j.tcb.2014.10.004

Strzyz, P. (2016). Post-translational modifications: extension of the tubulin code. *Nat. Rev. Mol. Cell Biol.* **17**, 609. doi:10.1038/nrm.2016.117

Wei, R. R., Al-Bassam, J. and Harrison, S. C. (2007). The Ndc80/HEC1 complex is a contact point for kinetochore-microtubule attachment. *Nat. Struct. Mol. Biol.* **14**, 54-59. doi:10.1038/nsmb1186

Welburn, J. P. I., Vleugel, M., Liu, D., Yates, J. R., Lampson, M. A., Fukagawa, T. and Cheeseman, I. M. (2010). Aurora B phosphorylates spatially distinct targets to differentially regulate the kinetochore-microtubule interface. *Mol. Cell* **38**, 383-392. doi:10.1016/j.molcel.2010.02.034

Wise, D., Cassimeris, L., Rieder, C. L., Wadsworth, P. and Salmon, E. D. (1991). Chromosome fiber dynamics and congression oscillations in metaphase Ptk2 cells at 23°C. *Cell Motil. Cytoskelet.* **18**, 131-142. doi:10.1002/cm.970180208

Wloga, D., Joachimiak, E. and Fabczak, H. (2017). Tubulin post-translational modifications and microtubule dynamics. *Int. J. Mol. Sci.* **18**, 2207. doi:10.3390/ijms18102207

Yu, I., Garnham, C. P. and Roll-Mecak, A. (2015). Writing and reading the tubulin code. *J. Biol. Chem.* **290**, 17163-17172. doi:10.1074/jbc.R115.637447

Zhai, Y., Kronebusch, P. J. and Borisy, G. G. (1995). Kinetochore microtubule dynamics and the metaphase-anaphase transition. *J. Cell Biol.* **131**, 721-734. doi:10.1083/jcb.131.3.721